WELDING RESEARCH

SUPPLEMENT TO THE *WELDING JOURNAL*, JUNE 2004
Sponsored by the American Welding Society and the Welding Research Council

Three-Dimensional Simulation of Transient GMA Weld Pool with Free Surface

A 3-D transient thermo-fluid model with free surface can analyze droplet flow effects on weld pool formation and weld bead profile such as finger-like penetration and weld toe radius

BY Z. CAO, Z. YANG, AND X. L. CHEN

ABSTRACT. A 3-D transient numerical model was developed for simulation of gas metal arc (GMA) weld pools with free surface and droplet impact effects. This effort predicted a moving GMA weld pool by considering not only the heat transfer and fluid flow driven by surface tension gradient, electromagnetic force, buoyancy, and arc pressure, but also detailed information about droplet flow effects on a weld pool, its solidification, and weld bead shape. Due to its unique capacity in simulation of free surface, this model can be applied to various welded joints. In the present study, the model was used to simulate both bead-on-plate and T-joints with different welding positions. The simulated weld bead geometries were in good agreement with experimental measurements.

Introduction

There has been growing recognition of the fact that convection in the weld pool is one of the dominant phenomena contributing to the weld pool formation (Refs. 1–4). The fluid flow inside the weld pool affects the heat transfer in the weld pool, the uniformity of weld composition, and the final weld bead profile. Furthermore, the thermal cycles experienced by the heat-affected zone during a welding operation determine solid-state transformations, thereby influencing the microstructure. In addition, weld bead profile is one of the critical factors in the specification for welded joint design, since it has a direct influence on welded structure stresses, weld joint strength, and fatigue life. Therefore, it is crucial to establish an accurate thermo-fluid model to simulate the entire welding thermal and fluid processes to obtain the desired weld bead profile and thermal history for structurally sound and high-performance welded joint design.

The gas metal arc welding process is one of the most commonly used joining methods because of its high productivity and process robustness. During GMA welding, weld metal is deposited into a weld pool from an electrode as a droplet stream. The metal transfer mechanisms play an important role in determining the resulting heat and fluid flow characteristics and final weld profile. The heat content and impact force of droplets tend to induce a series of physical, chemical, and metallurgical changes in the weld pool. Therefore, it is difficult to simulate the GMA welding process, mainly due to the droplet impact and the large flow and temperature gradients associated with this process. A better understanding of droplet impact effects on weld heat transfer and fluid flow is critical to determine welding procedures and to predict weld bead profiles.

To date, most investigations of fluid flow in weld pools have concentrated on the gas tungsten arc (GTA) welding processes, without including the complexity of metal transfer across the plasma (Refs. 5–12). Unfortunately, little work has been done in the area of fluid flow and heat transfer in GMA weld pools, due to its complexity. For instance, in Tsao's 2-D GMA weld pool model (Ref. 13), droplet heat was considered, but a flat weld pool surface was assumed. Weld pool surface deformation was incorporated in Kim's 3-D GMA weld pool solution (Ref. 14), while the effect of droplets was ignored. In another paper by Kim (Ref. 15), the droplet effect was taken into account. It was assumed that the molten droplet is transferred to the weld pool surface with distributed velocities of the Gaussian type. In Ohring's paper (Ref. 16), a 3-D transient GMA weld pool model was established by incorporating droplet and moving arc effects. However, the droplet influence was simulated by using a liquid column acting directly under the welding arc center with a constant impact speed. Apparently this kind of liquid column is very different from the individual droplets, unless these droplets transfer into the weld pool at an infinitely fast frequency. Recently, Davies (Ref. 17) proposed an investigation of the interaction of molten droplets with a liquid weld pool surface, but the model considered a 2-D stationary arc and did not incorporate arc travel effects. Yang and DebRoy (Ref. 18) considered the effect of droplets on GMA weld pool formation by incorporating a cylindrical volumetric heat source in the weld pool. The dimensions of the cylindrical volumetric heat source were calculated using parameters such as the drop size, shape, velocity, and frequency. Although their model demonstrated its capability to predict some essential features of GMA weld profile, such as finger penetration, the model was based on a fixed flat surface and cannot predict the metal reinforcement from GMA welding. In the author's recent paper (Ref. 19), a 3-D quasi-steady state model was proposed to describe fluid flow and heat transfer in a fully penetrated GMA weld pool. Droplet heat content, impact force, arc pressure, and pool surface deformation were considered. However, droplets were treated purely as a heat and momentum problem, and droplet effects on the fluid flow field in the weld pool were neglected.

KEYWORDS

Gas Metal Arc Welding
Modeling
Weld Pool
Fluid Flow
Heat Transfer
Free Surface
Droplet
T-Joint Fillet Weld

Z. CAO is with the Center for Welded Structures Research, Battelle Memorial Institute, Columbus, Ohio. Z. YANG and L. X. CHEN are with the Technical Center, Caterpillar Inc., Peoria, Ill.

It should be pointed out that all the aforementioned studies were focused on head on plate, and no 3-D transient computational fluid dynamics (CFD) models considering individual droplet impact and T-joints were reported for GMAW. In this study, a 3-D transient weld pool model was developed to study the fluid flow and heat transfer in the GMA welding process with consideration of individual droplets with high speed and high temperature. Both bead-on-plate and T-fillet joints at different positions were investigated, and experimental measurements were performed to validate the model.

Model Definition and Formulation

In order to simplify the mathematical model, the following assumptions have been adopted: 1) the flow is Newtonian and laminar, and compressibility is only included through the buoyancy term and the Boussinesq approximation; 2) physical properties, as listed in Table 1, are constant with temperature; and 3) the arc is regarded as a spatially distributed source of heat, current, and pressure flux.

Governing Equations

The coordinate system (x, y, z) is shown in Fig. 1. The workpiece bottom surface is used to define the x-y plane and the torch travels along the x-axis. A three-dimensional transient model is used to analyze the heat transfer and fluid flow for the GMA welding process. The computation domain is established to include the interaction of metal droplets with the weld pool. A moving arc and a fixed coordinate system are adopted for solving the transient problem. The metal droplets were generated as source term in the computation domain. It is assumed that spherical droplets at a certain height transfer into the weld pool. The droplets carry mass, momentum, and thermal energy, and periodically impinge into the weld pool. The initial temperature of the droplet is assumed to be constant. The droplet is also given an initial transfer speed, together with a horizontal speed with the welding torch. Once a droplet reaches the weld pool surface, the droplet interacts with the weld pool by transferring mass, momentum, and energy (Ref. 20). The values for droplet size (R_d), velocity (V_d), and its transfer frequency (F_d) are given in the appendix.

The heat transfer and fluid flow were calculated by numerical solution of the equations of conservation of mass, momentum, and energy in three-dimensional form. The governing equations are given as Equations 1–3. The mathematical equations provided in this section are valid for whole computation domain, which includes droplet, weld pool, and base material.

The value and physical meaning of each variable are listed in the appendix.

Mass continuity equation:

$$\nabla \cdot \vec{V} = 0 \tag{1}$$

Momentum equation:

$$\frac{\partial \vec{V}}{\partial t} + (\vec{V} \cdot \nabla)\vec{V} = \frac{1}{\rho}(\nabla p + \mu \nabla^2 \vec{V} + F_b) \tag{2}$$

Energy equation:

$$\frac{1}{\rho}\left[\frac{\partial h}{\partial t} + (\vec{V} \cdot \nabla)h\right] = \nabla \cdot (K \nabla T) \tag{3}$$

where

$$h = C_p \cdot T + f \cdot L$$

$$f(T) = \begin{cases} 0, \text{ if } T \le T_s \\ \dfrac{T - T_s}{T_l - T_s}, \text{ if } T_s < T < T_l \\ 1, \text{ if } T \ge T_l \end{cases} \tag{4}$$

The body force is calculated using the electromagnetic and buoyancy forces:

$$F_b = \vec{J} \times \vec{B} - \rho\beta\vec{g}\left(T - T_m\right) \tag{5}$$

The electromagnetic force in the present work is calculated based on Tsao's analytical solutions (Ref. 13).

Arc pressure is determined using the following formula (Ref. 21):

$$P_{arc}(x,y) = \frac{\mu_0 I^2}{4\pi^2 \sigma_j^2} \exp\left(-\frac{r^2}{2\sigma_j^2}\right) \tag{6}$$

It should be pointed out that the arc pressure in Equation 6 is adopted from the GTA welding process due to the lack of an arc pressure expression for GMA welding.

Table 1 — Parameters Used in Calculation

K	32.3 (solid)	W/m K
	26.9 (liquid)	W/m K
C_p	732	J/kg K
ρ	6900	kg/m^3
μ	5×10^{-3}	kg/m s
μ_o	1.26×10^{-6}	H/m
γ	1	N/m
γ_T	-0.2×10^{-3}	N/m K
β	1.0×10^{-4}	K^{-1}
T_v	2900	K
T_l	1798	K
T_s	1768	K
h_c	100	W/m^2 K
L_f	2.77×10^5	J/kg
L_c	7.34×10^6	J/kg
L	1.27	cm
σ_q	0.4	cm
σ_j	0.2	cm
u_o	0.5	cm/s
I	210	A
V	30	V
V_d	50	cm/s
F_d	400	drops/s
R_d	0.05	cm

Table 2 — Experimental Conditions

Material	A36 steel
Thickness	1.27 cm
Wire stickout	2.2 cm
Wire diameter	0.132 cm
Wire feed rate	13.76 cm/s
Welding current	280 A
Welding voltage	30 V
Welding speed	0.5 cm/s

Boundary Conditions

The boundary conditions for temperature distribution and fluid flow are described below:

a) Weld pool top surface

$$K\frac{\partial T}{\partial n} = \frac{\eta I V}{2\pi\sigma_q^2}\exp\left(-\frac{x^2+y^2}{2\sigma_q^2}\right) - h_c \cdot \left(T - T_o\right) - \sigma\varepsilon\left(T^4 - T_o^4\right) - q_{vap} \tag{7}$$

$$-p + 2\mu\frac{\partial V_n}{\partial n} = -p_{arc} + \frac{\gamma}{R}$$

$$\mu\frac{\partial V_\tau}{\partial n} = \gamma_T \frac{\partial T}{\partial \tau} \tag{8}$$

b) Bottom surface

$$K\frac{\partial T}{\partial n} = -h_c \cdot \left(T - T_o\right) - \sigma\varepsilon\left(T^4 - T_o^4\right)$$

$$u = v = w = 0 \tag{9}$$

c) Front surface

$$T = T_\infty$$

$$u = v = w = 0 \tag{10}$$

d) Rear and side surfaces

$$K\frac{\partial T}{\partial n} = -h_c \cdot \left(T - T_o\right) - \sigma\varepsilon\left(T^4 - T_o^4\right)$$

$$u = v = w = 0 \tag{11}$$

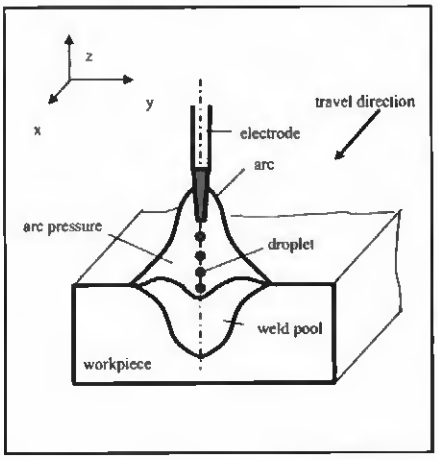

Fig. 1 — Schematic sketch of GMA welding.

Numerical Method

The developed weld thermo-fluid model in this research used a software package, *FLOW-3D* (Ref. 22), as the solver of the heat transfer and fluid flow in the weld pool. The selected solver has the capability of modeling fluid flow with free surface, which is a must to predict non-flat weld bead shape. A unique technique called the FAVOR (fractional-area-volume-obstacle-representation) method is used to define general geometric regions within the rectangular grid. Its free griding feature eliminates the tedious tasks of generating body-fitted or finite-element grids. Furthermore, this feature makes it possible to simulate the dynamic weld pool with free surface within a reasonable computation time frame. The flow region is subdivided into a mesh of fixed rectangular cells. With each cell, there are associated local average values of all dependent variables. All variables are located at the centers of the cells except for velocities, which are located at the cell faces (staggered grid arrangement). Curved weld surfaces (both molten and solidified) and other geometry features are embedded in the mesh by defining the fractional face areas and fractional volumes of the cells that are open to flow (Ref. 23). To construct discrete numerical approximations to the governing equations, control volumes are defined surrounding each dependent variable location.

Result and Discussion

A 3-D transient weld pool dynamics model is constructed to simulate the GMA welding process. The governing equations, including continuity, momentum, and energy equations, are discretized using the control volume method. The regular rectangle meshes are used in the whole domain. Convection, radiation, and evaporation are incorporated as thermal boundary conditions. Both droplet travel speed and arc pressure are involved to determine fluid flow field and free surfaces. Furthermore, latent heat of fusion and evaporation are considered in the model.

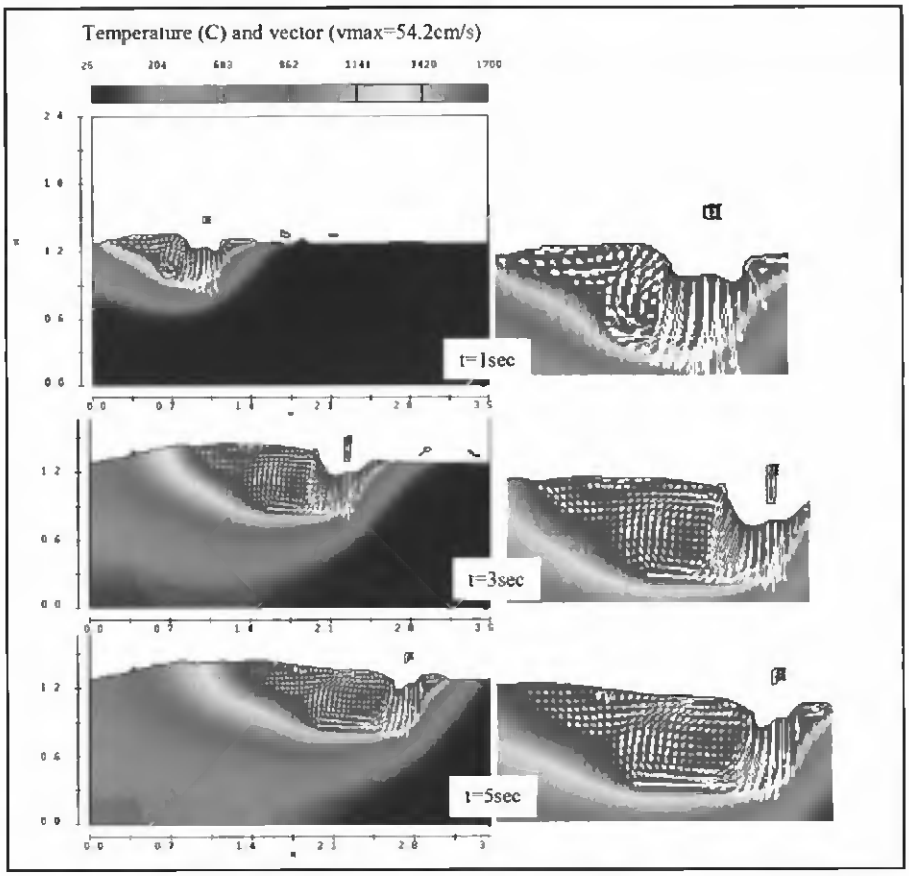

Fig. 2 — Temperature and fluid flow field at longitudinal cross section at different moments for the bead-on-plate case.

Three cases were analyzed in the study, which include bead-on-plate, horizontal-vertical T-joint, and T-joint with 45 degrees. The welding parameters used in experiments are given in Table 2. Other parameters and constants for simulation have been listed in Table 1.

Bead on Plate

The calculated temperature distribution and fluid flow field at different sections and at different moments for the bead-on-plate case are displayed in Figs. 2–4. The dark color at the middle indicates above-melting temperature, and the small arrows inside the weld pool represent molten material flow direction and magnitude. It can be seen that the weld pool penetration is developed gradually as welding time increases. As droplets enter the weld pool, both deep pool surface depression under the arc and high elevation away from the arc are clearly observed. The deposit material forms big weld reinforcement behind the welding torch.

In the longitudinal central cross section in Fig. 2, the three figures on the left side show temperature and fluid flow fields, and the three figures on the right show enlarged local views of their counterparts from the left side. It is seen that the weld pool depth does not change much after three seconds, which means the majority of penetration happens in the first three seconds, since the high-speed droplets penetrate the pool so quickly that this kind of penetration reaches equilibration after three seconds between the pool and droplets. As for fluid flow inside the weld pool, Fig. 2 (left side) shows a complex flow pattern in the weld pool. There exist two flow loops at the longitudinal cross section at all three moments. The big radially inward flow loop is dominated by the high-speed droplets and electromagnetic force. This is the driving force for GMA to form a deeply penetrated weld. The small radially outward flow loop behind the former one is driven by the surface tension gradient, and it makes the weld pool longer.

In order to capture the temperature and fluid flow features at the top view, results at the two cross sections (*A–A* is z = 1.25 cm for the left three figures, and *B–B*

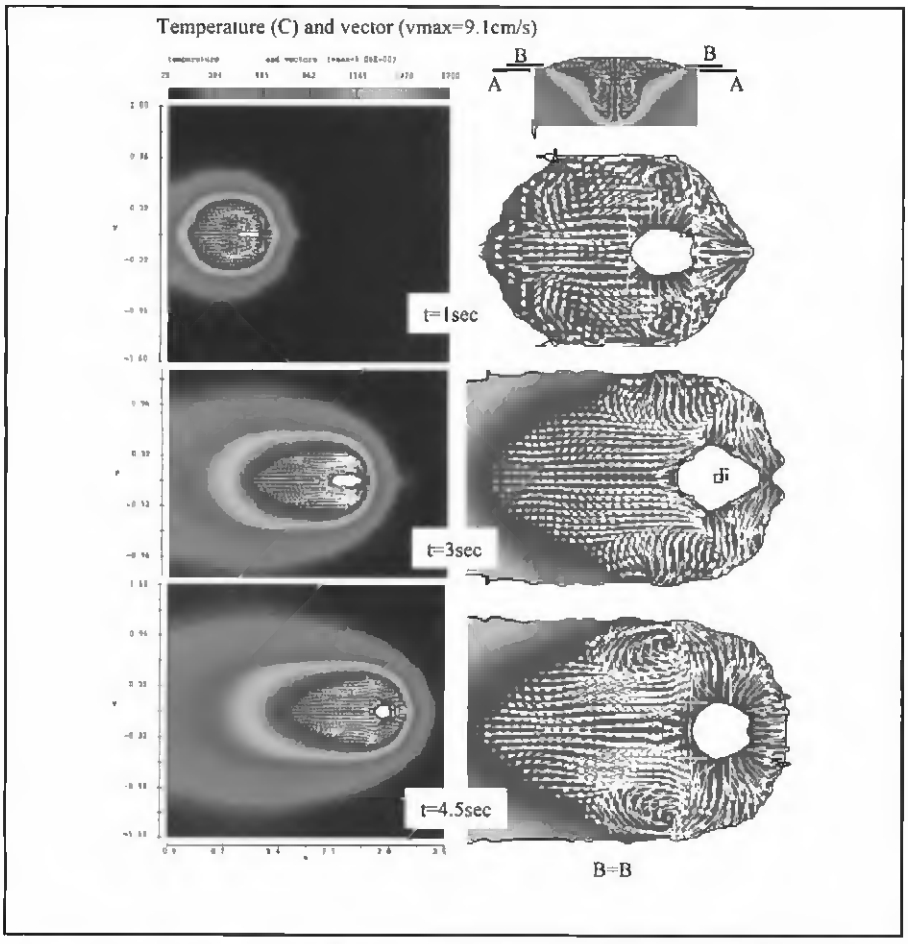

Fig. 3 — Temperature and fluid flow field at z = 1.25 cm cross section at different moments for the head-on-plate case.

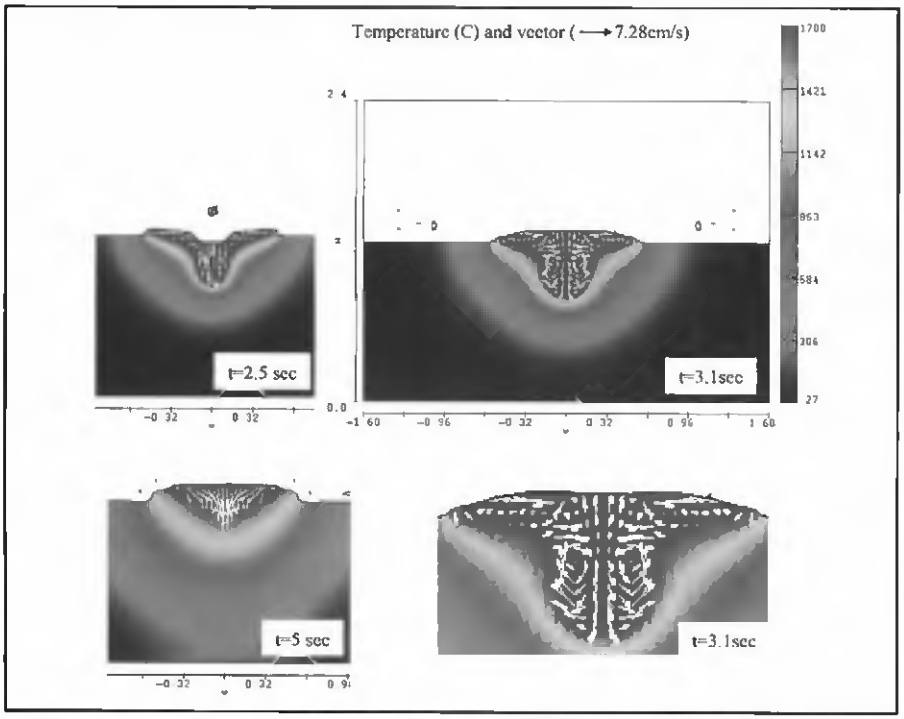

Fig. 4 — Temperature and fluid flow field at transverse cross section at different moments for the head-on-plate case.

is z = 1.29 cm for the right three figures) are plotted in Fig. 3. Since the plate thickness is 1.27 cm, only weld reinforcement is sectioned at *B–B*. From the top view, the weld pool is elliptical at the beginning, and then it gradually becomes a teardrop shape, due to the small radially outward flow loop mentioned at the longitudinal cross section. Also, it is because the part of the weld pool behind the torch still holds higher than melting temperature, and the part of the weld pool directly under the torch is continuously heated. This type of teardrop-shaped weld pool was observed by Kou (Ref. 24) for high heat input and high travel speed. Also, it can be seen that there are two small flow loops behind the arc near the weld interface. They are caused by the strong backward flow, and are contributing to enlarging the weld width.

From the transverse cross section in Fig.4, it is found that the deepest penetration occurs at the section when the arc reaches the surface. Reinforcement forms after the arc passes. Fluid at the cross section when t = 2.5 s flows downward at the center driven by droplet flow, and flows outward driven by the surface tension gradient. This trend can be observed more clearly at the cross section when t = 3.1 s. Deep inside the pool, there are two downward flow loops, which produced deep and finger-like penetrations. Near the pool surface, there are two outward flow loops, which generated wide pool width.

Figure 5 shows the 3-D temperature distribution of the head-on-plate case. The half model is displayed because of its symmetrical features. It can be seen that the splatter of droplets is severe at the beginning, and the situation of splatter is improved as time increases. The weld head is formed uniformly along the welding direction, and the weld bead shape can be observed. Under the given GMA welding condition, it can be observed that the droplet impact force, surface tension gradient force, and electromagnetic force are the predominant factors in determining weld pool penetration and fluid flow velocity and pattern. Weld penetration is primarily determined by the droplet impact force, while weld width is determined by surface tension gradient force. To justify this statement, we also did a simulation for another case with much lower droplet velocity (5 cm/s). The penetrations assuming two different metal droplet velocities are compared in Fig. 6. It is observed that the penetration from normal droplet velocity (50 cm/s), which was selected based on the data in literature, is significantly higher than that from assumed low droplet velocity (5 cm/s). As is shown later in Fig. 13A, the predicted weld penetration using 50-cm/s droplet velocity is comparable with

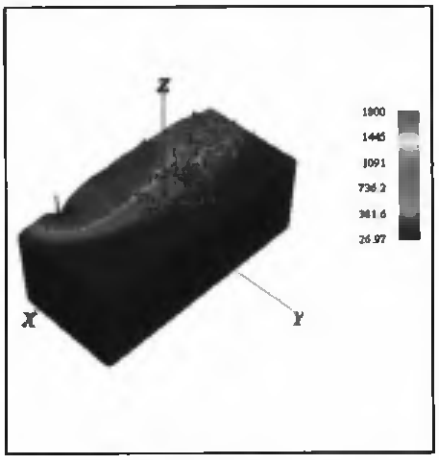

Fig. 5 — Three-dimensional temperature distribution for the bead-on-plate case.

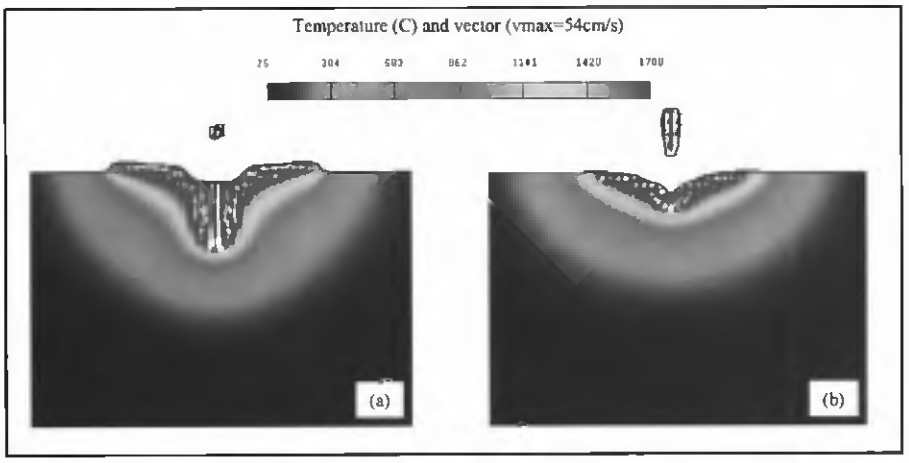

Fig. 6 — Comparison of calculated penetration assuming different metal droplet velocities: A — 50 cm/s; B — 5 cm/s.

the experimental results. In contrast, the predicted penetration using 5-cm/s droplet velocity is much lower than the actual penetration. Thus, it is clear that weld penetration is primarily determined by the metal droplet impact force. Compared to metal droplet impact force, the effect of electromagnetic force on weld penetration is much less under the investigated GMA welding condition. The finger-like penetration that occurs in GMA welding is caused by the combination of the droplet impact force, surface tension gradient, and electromagnetic force.

Horizontal-Vertical T-Joint

With a T-joint, unlike the bead-on-plate cases, there are both horizontal and vertical plates, and the arc torch has a 45-deg angle with respect to the horizon. In order to compare the joint type effects, all the calculation parameters used are the same as in the bead-on-plate case.

The calculated temperature distribution and fluid flow field at transverse cross sections and at different moments are displayed in Fig. 7. The arc center is located at the cross section when t = 2.5 s. As shown in Fig. 7A, finger-like penetration still occurs for this case, due to the combination of droplet impact force and electromagnetic force. The maximum velocity at this moment is 5.39 cm/s, which is a little larger than the specified velocity of a metal droplet. When the arc moves away from this location, as shown in Fig. 7B, the maximum velocity decreased to 0.729 cm/s. This is because surface tension gradient force at this moment is dominant at this location. Thus, the fluid near the pool surface flows from the center outward. In addition, more fluid is formed near the horizontal plate due to gravity. As a result, the leg length of the weld on the horizontal side is larger than that on the vertical

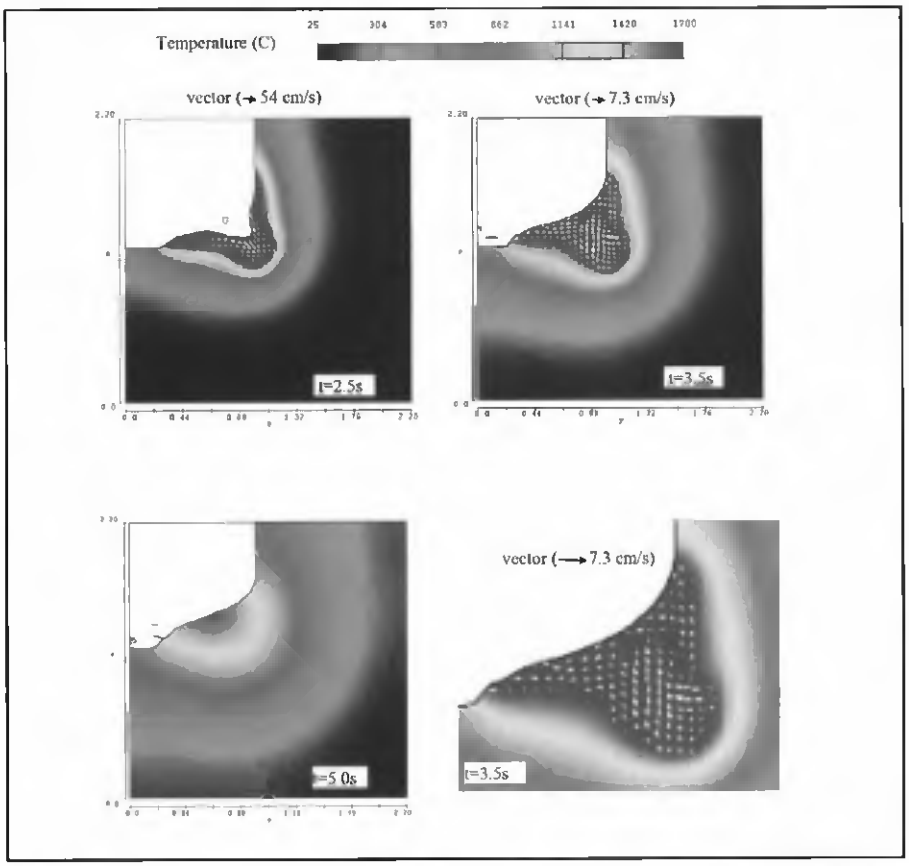

Fig. 7 — Temperature and fluid flow field at transverse cross section at different moments for the horizontal T-fillet case.

side. The predicted final weld bead shape after solidification is shown in Fig. 7C.

The calculated temperature distribution and fluid flow field at longitudinal cross sections and at different moments are displayed in Fig. 8. Since the longitudinal cross section is taken near the vertical plate surface, the weld reinforcement is naturally higher at this view. In the weld pool, there are two same-sized flow loops overlapping each other. The top loop, driven by surface tension gradient, flows outward at the pool surface; and the bottom loop, driven by droplet impact and electromagnetic force, flows downward deep inside the pool.

The three-dimensional temperature distribution is shown in Fig. 9. It can be observed that there is severe spatter at the beginning of the weld, and some spatter is

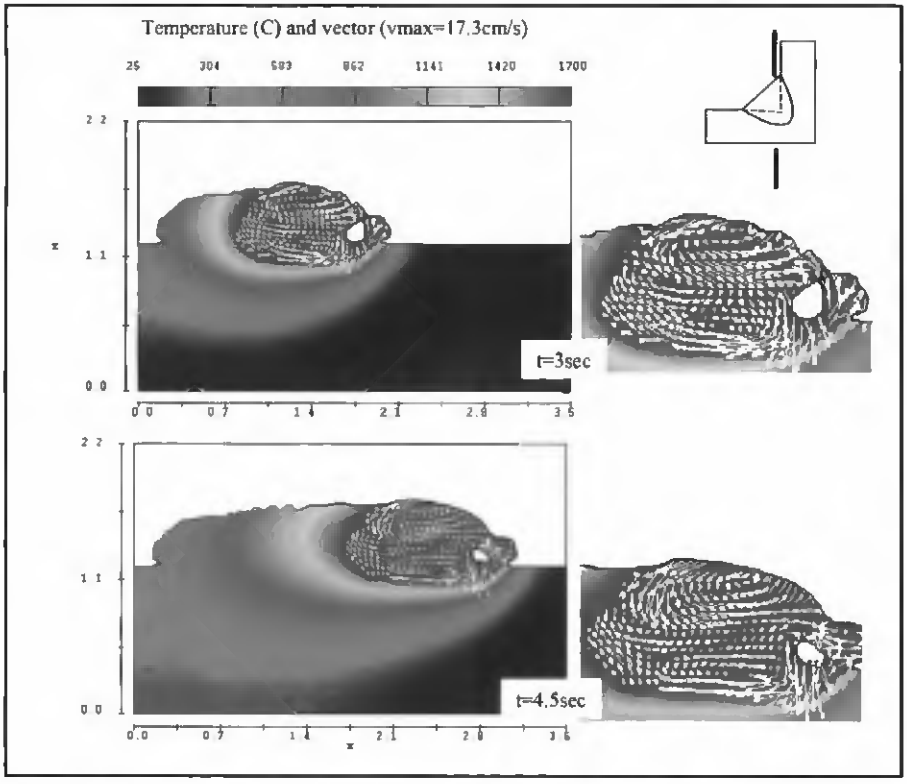

Fig. 8 — Temperature and fluid flow field at longitudinal cross section at different moments for the horizontal T-fillet case.

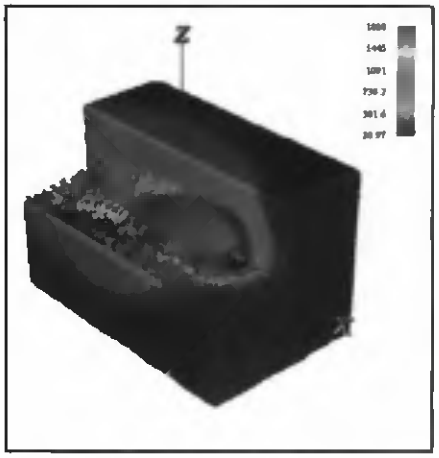

Fig. 9 — Three-dimensional temperature distribution for the horizontal T-fillet case.

located on the side of the weld on the horizontal plate. However, the situation is improved when time increases. Also, the weld bead shape can be observed clearly.

T-Joint with 45 Degrees

In this case, the horizontal-vertical T-joint structure from the last case is rotated 45 deg around the *x*-axis, so that the weld torch is located at the vertical position and it has the same angles (45 deg) to the two plates. The calculated temperature distribution and fluid flow field at longitudinal and transverse cross sections and at different moments are displayed in Figs. 10 and 11, respectively. There is much splatter in the torch travel direction, and less splatter along the side of the weld, which is due to its special joint position.

Figure 11 shows that both the weld surface and the transition between weld and plate are very smooth. Obviously, this is more desirable than those of the horizontal-vertical T-joint from the fatigue point of view. Finger-like penetration occurs again for this case, due to the high-speed droplet flow (which increases the penetration) and the two outward flow loops beside the weld center (which increase the weld width).

From Fig.11, the weld reinforcement is also higher at this view than that in the bead-on-plate case in Fig. 2. However, the fluid flow patterns at these longitudinal cross sections are similar to those in the bead-on-plate case in Fig. 2, except that the flow loop driven by droplet impact and electromagnetic force is much bigger than that in Fig. 2. The three-dimensional temperature distribution is shown in Fig. 12. Only half of the model is plotted, due to the symmetrical features of the structure. Again, the weld bead shape can be observed clearly from this view. Some splat-

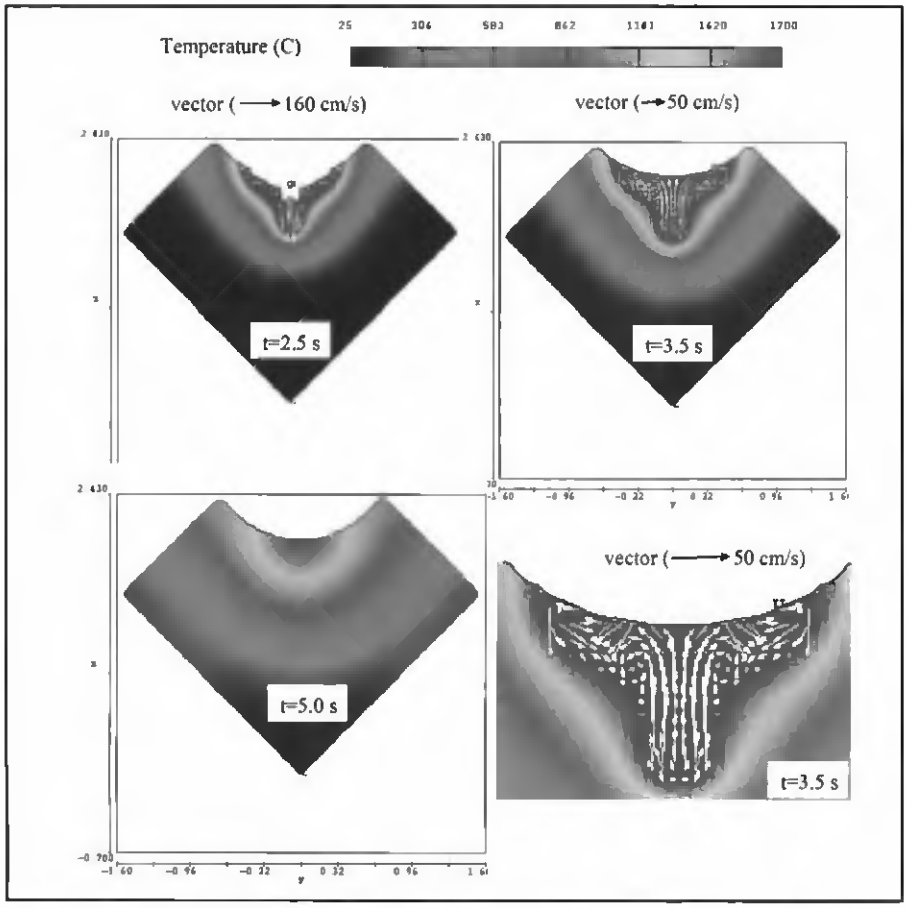

Fig. 10 — Temperature and fluid flow field at transverse cross section at different moments for the 45-deg T-joint case.

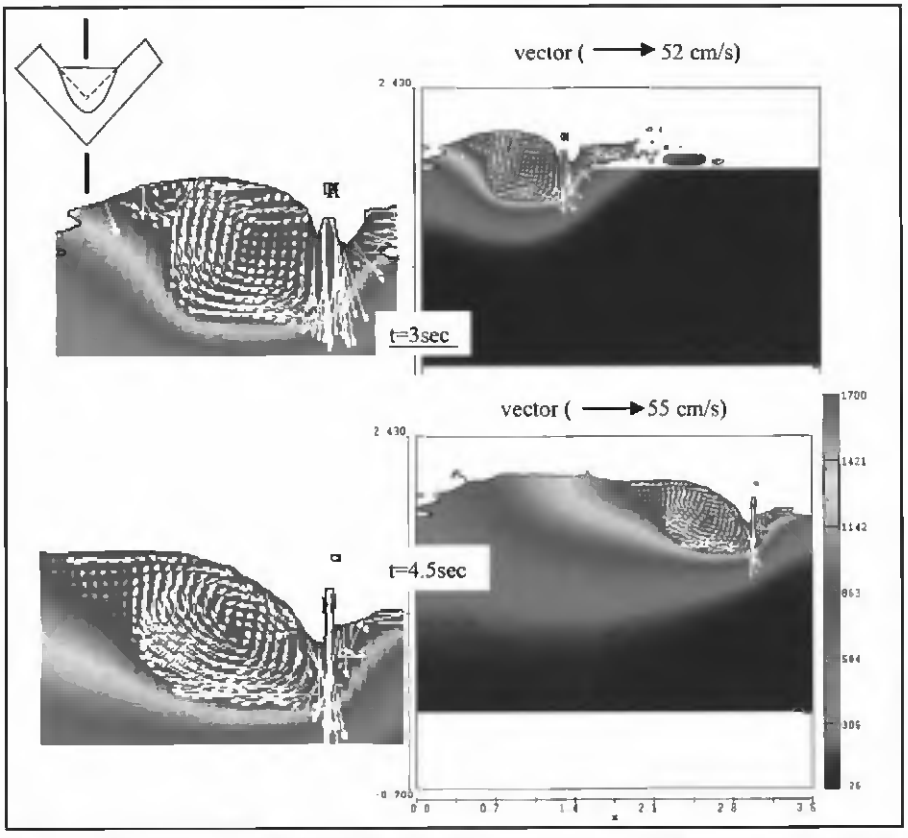

Fig. 11 — Temperature and fluid flow field at longitudinal cross section at different moments for the 45-deg T-joint case.

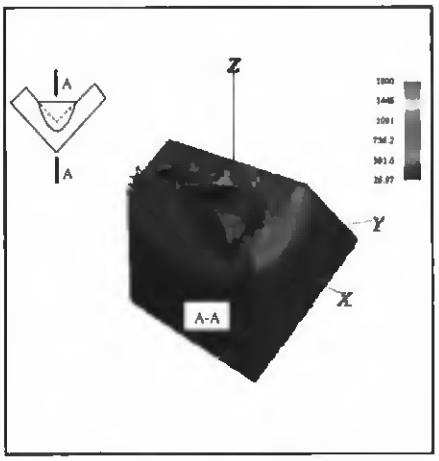

Fig. 12 — Three-dimensional temperature distribution for the 45-deg T-joint case.

ter can be seen, but it is less severe than the horizotal-vertical case in Fig. 9 and, especially, the weld bead shape is better.

Validation

To validate the modeling results, GMA welding experiments were carried out for both bead-on-plate and T-fillet welds. The test conditions are listed in Table 2. Comparisons between the calculated and actual weld bead shape for both bead-on-plate and T-fillet welds are shown in Fig. 13. It can be seen that the predicted weld width and depth are close to the experimental ones in both cases. In the bead-on-plate case, the predicted width and depth are 0.124 cm and 0.039 cm, and the measured width and depth are 0.129 cm and 0.041 cm. Also, the finger-like penetration is captured from the prediction, and its penetration shape matches the experimental one well. In the T-fillet weld case, the concave weld bead shape was well predicted from simulation. As shown in Fig. 13B, the predicted penetration and weld toe radius are comparable with the actual weld geometry.

Concluding Remarks

A 3-D transient thermo-fluid model with free surface was developed to simulate the heat transfer and fluid flow in the GMA weld pool. This work represents the first effort to explicitly simulate the interaction of a metal droplet with the weld pool using the free surface model. The model has been used to analyze the heat transfer and fluid flow pattern for different types of welded joints, including bead-on-plate and T-fillet joints. The predicted weld bead shapes were compared with the experimental results. The results here in-

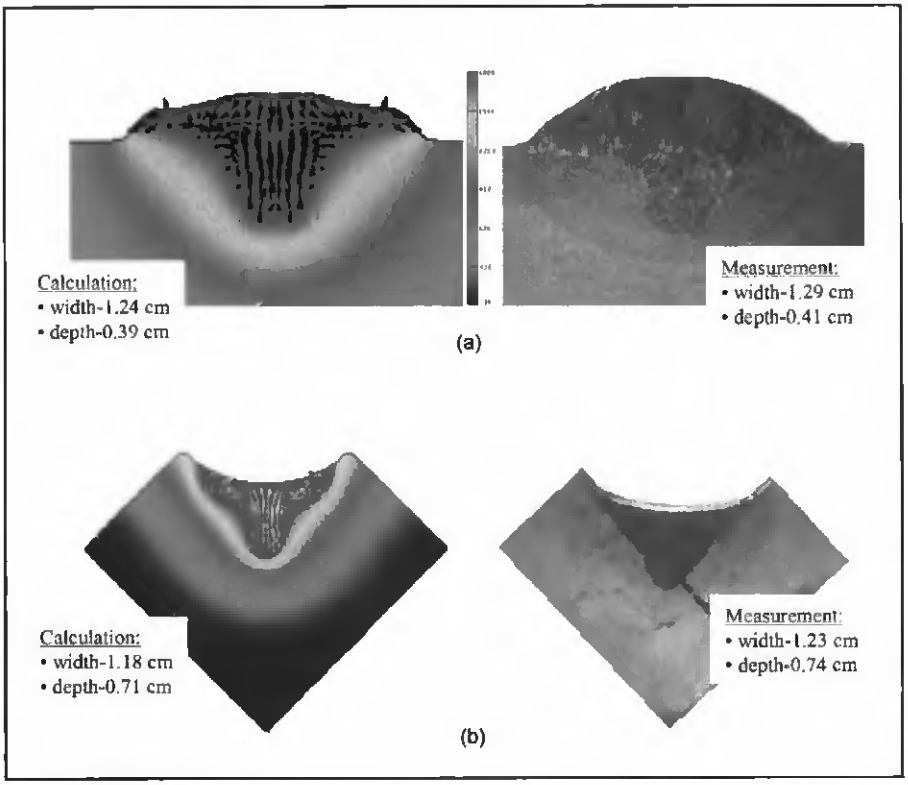

Fig. 13 — Weld profile comparison between calculation and measurement for: A — bead-on-plate; B — 45-deg T-fillet weld.

dicate the significant promise to use a 3-D transient free-surface weld thermo-fluid model to design a desired weld bead shape for a high-performance welded joint. The following conclusions can be made from the present work:

- The 3-D transient free-surface model can simulate the details for weld pool formation during the GMA welding process. This includes melting of base material, interaction of the metal droplet with the weld pool, weld pool solidification, and final weld bead shape.
- The flow pattern in the GMA welding process can be well predicted by considering the combined forces from metal droplet impact, surface tension gradient, electromagnetic force, arc pressure, and gravity. Among all of the forces, the metal droplet impact is the primary force responsible for penetration, which in combination with the outward flow on the pool surface driven by tension gradient force, causes the finger penetration in GMA welds.
- The 3-D free-surface model is capable of simulating heat transfer and fluid flow in various types of welds. The detailed features for GMA welds, such as finger penetration, reinforcement due to wire deposition, and weld toe, can be modeled. Good agreement was observed between the predicted and actual welds.

Acknowledgments

The authors would like to thank Dr. F. W. Brust and Dr. P. Dong of Battelle for their support and suggestions. This paper was prepared with the support of U.S. Department of Energy (DOE) Award Number DE-FC07-01ID14242. However, any opinions, findings, conclusions, or recommendations expressed herein are those of the authors and do not necessarily reflect the views of DOE.

References

1. Oper, G. M., and Szekely, J. 1984. Heat and fluid flow phenomena in weld pools. *Journal of Fluid Mechanics* 147:53–79.

2. Chan, C., Mazumder, J., and Chan, M. M. 1984. A two-dimensional transient model for convection in laser melted pools. *Metallurgical Transactions* 15A:2175–2184.

3. Kou, S., and Wang, Y. H. 1986. Computer simulation of convection in moving arc weld pools. *Metallurgical Transactions* 17A:2271–2277.

4. Zacharia, T., et al. 1989. Three-dimensional transient model arc welding process. *Metallurgical Transactions* 20B:645–659.

5. Heiple, C. R., and Roper, J. R. 1982. Mechanism for minor element effects on GTA fusion zone geometry. *Welding Journal* 60(8): 143-s to 145-s.

6. Thompson, M. E., and Szekely, J. 1989. The transient behavior of weld pools with a deformed free surface. *International Journal of Heat & Mass Transfer* 32(6): 1007–1019.

7. Choo, R. T. C., and Szekely, J. 1990. Modeling of high-current arc with emphasis on free surface phenomena in the weld pool. *Welding Journal* 69(9): 223-s to 233-s.

8. Tsai, M. C., and Kou, S. 1989. Marangoni convection in weld pools with a free surface. *International Journal of Numerical Methods in Fluid* 9:1503–1516.

9. Kim, S. D., and Na, S. J. 1992. Effect of weld pool deformation on weld penetration in stationary gas tungsten arc welding. *Welding Journal* 71(5): 179-s to 193-s.

10. Zhang, Y. M., Cao, Z. N., and Kovacevic, R. 1995. Numerical analysis of fully penetrated weld pools in GTA welding. *Proc. Instn. Mech. Engrs., Part C: Journal of Mechanical Engineering Science* 210:187–195.

11. Kovacevic, R., Cao, Z. N., and Zhang, Y. M. 1996. Role of welding parameters in determining the geometrical appearance of weld pool. *ASME Transactions Journal of Engineering Materials and Technology* 118(10): 589–596.

12. Cao, Z. N., Zhang, Y. M., and Kovacevic, R. 1998. Numerical dynamics analysis of moving GTA weld pool. *ASME Transactions Journal of Manufacturing Science and Engineering* 120(2): 173–178.

13. Tsao, K. C., and Wu, C. S. 1988. Fluid flow and heat transfer in GMA weld pool. *Welding Journal* 67(3): 70-s to 75-s.

14. Kim, S. -D., and Na, S. -J. 1995. A study on the effect of constant tube-to-workpiece distance on weld pool shape in gas metal arc welding. *Welding Journal* 74(5): 141-s to 152-s.

15. Kim, S. -D., and Na, S. -J. 1994. A study on the three-dimensional analysis of heat and fluid and flow in gas metal arc welding using boundary-fitted coordinates. *ASME Transactions Journal of Engineering for Industry* 116(2): 78–85.

16. Davies, M. H., Wahab, M., and Painter, M. J. 2000. Investigation of the interaction of a molten droplet with a liquid weld pool surface: A computational and experimental approach *Welding Journal* 79(1): 18-s to 23-s.

17. Ohring, S., and Lugt, H. J. 2000. Numerical simulation of a time-dependent 3-D GMA weld pool due to a moving arc. *Welding Journal* 78(12): 416-s to 424-s.

18. Yang, Z., and DebRoy, T. 1999. Modeling macro- and microstructures of gas-metal-arc welded HSLA-100 steel. *Metallurgical and Material Trans.* 30B: 483–488.

19. Cao, Z., and Dong, P. 1998. Modeling of GMA weld pools with consideration of droplet impact. *ASME Journal of Engineering Materials and Technology* 120(10): 313–319.

20. Wang, Y., and Tsai, H. L. 2001. Effects of surface active elements on weld pool fluid flow and weld penetration in gas metal arc welding. *Metallurgical and Material Trans.* 32B:501–515.

21. Tsai, N. S. and Eagar, T. W. 1985. Distribution of the heat and current fluxes in gas tungsten arcs. *Metallurgical Transactions* 16B:841–846

22. *FLOW-3D User's Manual, Excellence in Flow Modeling Software.* Version 7.7. Flow Science, Inc.

23. Hirt, C. W., and Sicilian, J. M. 1985. A porosity technique for definition of obstacles in rectangular cell meshes. *Proc. Fourth International Conf. Ship Hydro.* Washington, D.C.: National Academy of Science.

24. Kou, S., and Le, Y. 1988. Welding parameters and grain structure of weld metal — A thermal dynamic consideration. *Metall. Trans.* 19A:1075–1083.

Appendix

Nomenclature

$\vec{B}$	magnetic induction vector, tesla
C_p	specific heat, J/kgK
f	frequency of droplet transfer, 1/s
F_b	component of body force, N
$\vec{g}$	gravitational acceleration vector, m/s²
h_c	convection coefficient, W/m²K
I	welding current, A
$\vec{J}$	current density vector, A/m²
K	thermal conductivity, W/mK
L_f	latent heat of fusion
L_e	latent heat of evaporation
L	thickness
n	normal unit vector to outer pool surface
p	pressure, N/m²
P_{arc}	arc pressure, N/m²
q_{evap}	heat loss from evaporation, W/m²
r	radial distance, m
R	radius of surface curvature, m
T	temperature, K
T_∞	ambient temperature, K
T_m	melting temperature, K
T_v	boiling point
T_l	liquidus temperature
T_s	solidus temperature
u_0	welding speed, m/s
u	x-direction velocity, m/s
V	arc voltage, V
$\vec{V}$	velocity vector, m/s
V_τ	velocity component in surface tangential direction
V_d	droplet transfer velocity, m/s
V_n	velocity component in surface normal direction
v	y-direction velocity, m/s
w	z-direction velocity, m/s
x,y,z	coordinates, m
μ	viscosity, kg/ms
μ_0	magnetic permeability, H/m
ρ	density, kg/m³
ρ_d	droplet density, kg/m³
β	coefficient of volume expansion, 1/K
γ	surface tension, N/m
$\partial\gamma/\partial\gamma$	surface tension temp. coefficient, N/mK
η	arc efficiency
σ	Stefan-Boltzmann constant, 5.67×10^{-8} W/m²K⁴
σ_q	arc heat flux distribution parameter
σ_j	arc current flux distribution parameter
ε	surface emittance, 0.8
τ	the tangential direction of the pool surface